IEEE Access
Multidisciplinary | Rapid Review | Open Access Journal

Received 13 December 2024, accepted 24 December 2024, date of publication 31 December 2024, date of current version 10 January 2025.

Digital Object Identifier 10.1109/ACCESS.2024.3524630

RESEARCH ARTICLE

Flat-Panel-Rectenna With Broad RF Energy Harvesting Coverage for Wireless-Powered Sensor Applications

YAN HAN[1], EUNJI KIM[1], AND HAN LIM LEE[1,2], (Member, IEEE)
[1]Department of Intelligent Semiconductor Engineering, Chung-Ang University, Seoul 06974, South Korea
[2]School of Electrical and Electronics Engineering, Chung-Ang University, Seoul 06974, South Korea

Corresponding author: Han Lim Lee (hanlimlee@cau.ac.kr)

This work was supported in part by the Institute of Information and Communications Technology Planning and Evaluation (IITP) Grant funded by the Korea Government (MSIT) (Development of Envelope Tracking PAM for Sub-6GHz Massive MIMO Supported Base Stations) under Grant RS-2024-00395702 and in part by the Chung-Ang University Young Scientist Scholarship in 2023.

ABSTRACT To circumvent the issue of significant space occupation associated with omnidirectional antenna-based rectennas and to seamlessly integrate into self-powered applications with minimal uncovered zones, this paper presents a new flat-panel rectenna (FPR) designed specifically for microwave-based wireless power charged sensor applications. This innovation aims to optimize space efficiency and enhance energy capture capabilities, providing a more effective solution for the continuous and reliable operation of wireless powered devices in various sectors. The proposed compact rectenna is designed with a planar antenna featuring wide beamwidth and an RF-to-DC conversion network that includes a dual-voltage rectifier architecture and a customized matching network to optimize RF-to-DC conversion efficiency. The FPR is then integrated with a batteryless heart rate sensor, enabling the sensor to operate and expand its physical orientation while maintaining accurate monitoring. The performance of the proposed RF energy harvester was evaluated at 5.8 GHz, showing a half-power coverage of 144.6° with respect to a peak antenna gain of 3.34 dBi, and a peak RF-to-DC conversion efficiency of 51.8%. Additionally, the batteryless sensor was shown to function effectively with a maximum RF energy incident angle of 140°, despite the flat-panel architecture.

INDEX TERMS Rectenna, RF energy harvester, self-powered sensor, wireless-powered sensor, wireless power transmission.

I. INTRODUCTION

The emergence of wireless power charging (WPC) through radio frequency (RF) energy harvesting marks a significant technological advancement, enabling an uninterrupted power supply for various low-power applications in the Internet of Things (IoT) environment. At the core of RF energy harvesting technology is the rectenna, a device designed to convert RF signals into direct current (DC). While early research focused on maximizing energy conversion efficiency and extending transmission range, the increasing adoption of RF energy harvesting has spurred novel approaches and the fast development of smart applications across industrial, medical, and consumer electronics sectors. These advancements include the introduction of rectenna arrays to improve RF-to-DC conversion efficiency and the development of broadband rectennas optimized for low input power levels. Efforts have also been made to integrate filters between the rectifier and antenna to reduce RF signal reflection and minimize the impact of higher-order harmonics. However, a research gap remains in optimizing rectennas for wide-angle energy reception, feature increasingly critical for ultra-low power IoT sensors and self-powered applications, where the inevitable misalignment of mobile devices can significantly affect performance. Recent initiatives have led to the development of rectennas capable of dissecting RF signals into in-phase and

The associate editor coordinating the review of this manuscript and approving it for publication was Li Yang.

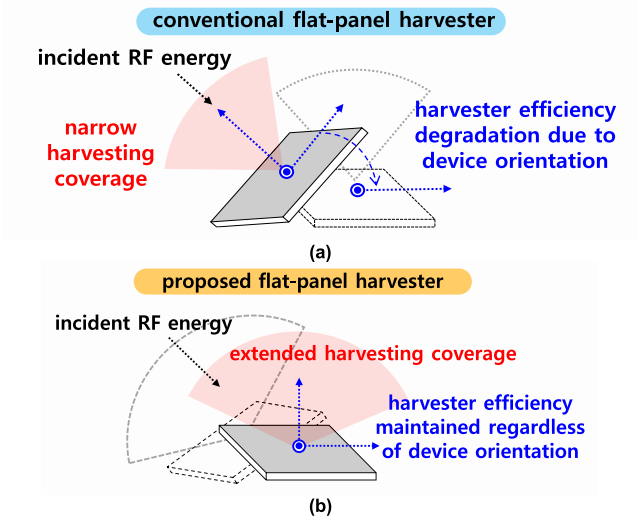

FIGURE 1. Flat-panel RF energy harvester with (a) conventional patch-based rectenna coverage and (b) proposed rectenna coverage.

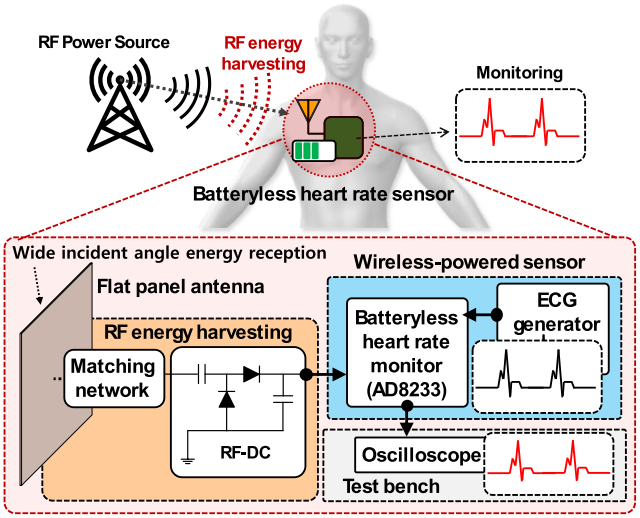

FIGURE 2. Proposed flat panel RF energy harvester embedded heartrate monitor application.

anti-phase components, achieving wide-angle reception [1], [2]. However, the use of magic-T based RF signal partitioning device reduces the compactness of the rectenna, requiring a larger ground plane. Additionally, it only enhances the reception of RF signals in the E-plane or H-plane, significantly limiting the rectenna's operational performance. Innovations also include wide-angle rectennas that utilize triple-feed array antennas [3], [4]. The output voltage can be combined in DC using parallel-connected Schottky diodes, enabling wide-angle reception in both the E- and H-planes. However, only a 60° coverage can be achieved, which falls short of meeting the omni-directional requirements of emerging ultra-low power IoT applications. To improve signal conversion efficiency and optimize energy reception over a wide range of incident angles, rectenna arrays paired with beam-forming matrices and related DC power management networks have been proposed [5], [6], [7], [8], [9]. However, the overall size of the rectenna inevitably increases due to the addition of extra circuit modules, and it is only the capability of signal reception at horizontal azimuth direction is enhanced. If they are not directed toward the intended source at elevation direction, it has a drastic power decrease. Several methods have been explored to enhance rectenna performance, including the use of a series-coupled patch array to eliminate complex circuit modules [10], [11] and the transformation from linear to circular polarization to achieve a wide beamwidth [12]. Nevertheless, these rectennas either have high-profile, non-planar structures or suffer from low gain, limiting their practical application. The development of compact rectennas with wide coverage is crucial, as it marks a significant step toward making wireless power charging through RF energy harvesting more versatile and applicable across a broader range of scenarios.

Recently, planar-type wide beamwidth antenna elements and array antennas have been proposed by the authors' group [13], [14]. Although these structures have demonstrated efficacy in increasing communication coverage for phased array applications, their feasibility in self-powered sensor applications have not yet been investigated. This paper aims to bridge that research gap by focusing on the enhancement and optimization of wide beamwidth-based rectennas, ensuring they are well-suited to meet the demands of WPC and wireless self-powered sensor operation. In this paper, we propose a compact flat-panel rectenna (FPR), which can be distinguished from the conventional patch-based architecture, as shown in Fig. 1(a) and (b). The main contribution of this paper is to demonstrate improved flexibility in the physical orientation of RF energy harvester-embedded devices. The conventional architecture shown in Fig. 1(a) exhibits limited coverage, leading to interruptions in WPC due to its physical orientation. However, the proposed FPR ensures reliable RF-to-DC conversion regardless of device orientation, thanks to its extended beam coverage, as illustrated in Fig. 1(b). Furthermore, the proposed FPR is integrated with a low-power heart rate monitoring sensor, demonstrating the feasibility of a practical self-powered sensor solution as described in Fig. 2. Specifically, this paper is organized as follows: Section II introduces the design methods for the antenna element and rectifier of the proposed FPR, respectively. Section III verifies the performance of the proposed rectenna and the self-powered sensor at various incident angles of RF energy. Lastly, Section IV concludes this paper.

II. DESIGN AND ANALYSIS OF THE PROPOSED FLAT PANEL RECTENNA

A. DESIGN OF WIDE-ANGLE FLAT-PANEL ANTENNA

In general, the wide-coverage attribute of a rectenna is primarily achieved through its antenna component, so the analysis begins with the conventional patch antenna configuration, as shown in Fig. 3(a). In this configuration, L_e, W, and h

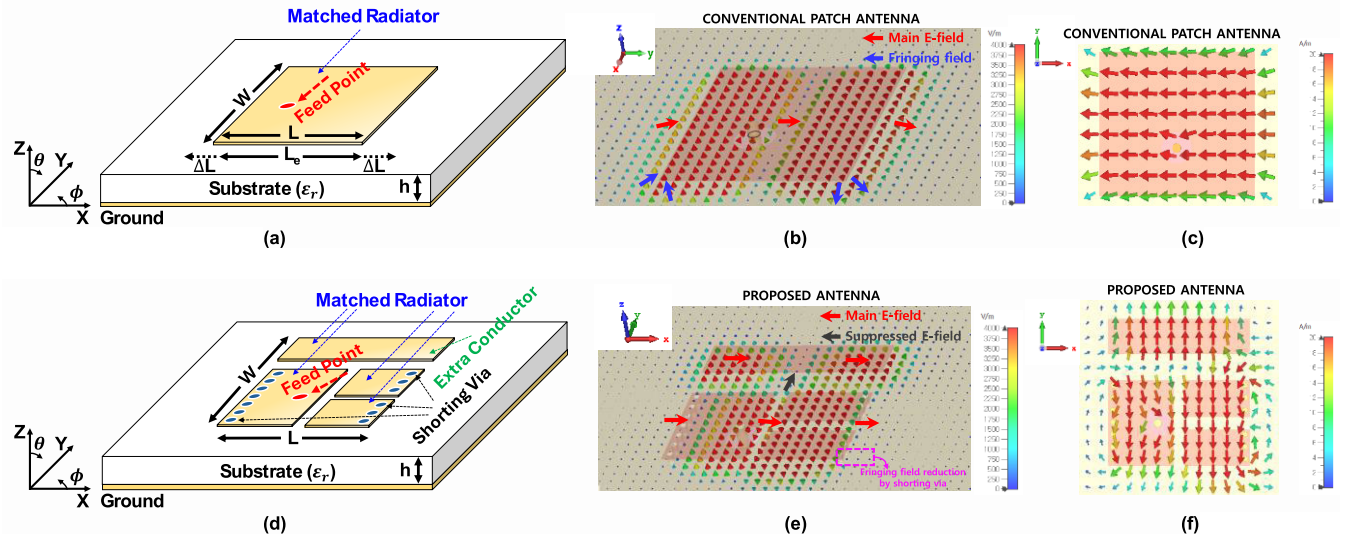

FIGURE 3. Planar antenna analysis of (a) patch-type with (b) simulated E-field and (c) simulated H-field, and (d) proposed type with (e) simulated E-field and (f) simulated H-field.

represent the effective electrical length of patch, the width of patch, and the thickness of the substrate respectively. The normalized E-field pattern of the conventional patch antenna can then be approximately estimated as follows [15],

$$E_\theta(\theta,\phi) = \frac{\sin\left(\frac{\pi(W)}{\lambda}\sin\theta\sin\phi\right)}{\frac{\pi(W)}{\lambda}\sin\theta\sin\phi} \cdot \cos\left(\frac{\pi(L_e)}{\lambda}\sin\theta\cos\phi\right)\cos\phi \quad (1)$$

and

$$E_\phi(\theta,\phi) = -\frac{\sin\left(\frac{\pi(W)}{\lambda}\sin\theta\sin\phi\right)}{\frac{\pi(W)}{\lambda}\sin\theta\sin\phi} \cdot \cos\left(\frac{\pi(L_e)}{\lambda}\sin\theta\cos\phi\right)\cos\theta\sin\phi \quad (2)$$

where θ and ϕ are the elevation and azimuth angles respectively. It is observed that the beam pattern is pertinent to the resonance frequency wavelength, effective length and width of the patch, which are expressed as λ, L_e L_e and W. Due to the fringing fields, L_e is relevant to patch length L, which can be expressed as follows,

$$L_e = L + 2\Delta L. \quad (3)$$

Furthermore, the normalized E-field pattern in E-plane can be deduced as follows [15],

$$E_\theta(\theta,0)_E = \cos\left(\frac{\pi(L_e)}{\lambda}\sin\theta\right). \quad (4)$$

And the normalized E-field pattern in H-plane can be further deduced as follows,

$$E_\phi\left(\theta,90^\circ\right)_H = -\frac{\sin\left(\frac{\pi(W)}{\lambda}\sin\theta\right)}{\frac{\pi(W)}{\lambda}\sin\theta}\cos\theta. \quad (5)$$

According to equations (4) and (5), the width of the patch is directly proportional to the beamwidth, while the effective length of the patch is inversely proportional to the beamwidth. Based on equation (3), the key to increasing beamwidth lies in reducing the influence of fringing fields and expanding the patch width. To visualize the fringing fields, the reference patch antenna was designed with a ground size of 1.1 $\lambda_0 \times 1.1\ \lambda_0$. The substrate used is Taconic TLX-9, which has a relative permittivity, ε_r, of 2.5 and a loss tangent of 0.0019. Fig. 3(b) and (c) show the E-field and H-field distributions of the conventional patch antenna, respectively. The 3D electromagnetic (EM) simulation of the conventional patch antenna's E-field confirms the presence of fringing fields, which make the effective length of the patch larger than its physical length, thereby limiting the antenna's beamwidth. To improve the beamwidth in both planes, the width of the patch was first increased to achieve a larger half-power beamwidth (HPBW) in the H-plane. This expansion was accomplished by using multiple segmented conductors with shorting vias, as shown in Fig. 3(d). Dividing the single patch into several segments introduced additional capacitance, so shorting pins were added to provide extra inductance, ensuring proper impedance matching at the operating frequency. Furthermore, the inclusion of shorting pins in the center conductors canceled the E-field, which suppressed the fringing field at the resonance frequency, as depicted in Fig. 3(e). Fig. 3(f) also shows the simulated H-field associated with the E-field generation. As a result, the beamwidth in the E-plane was expanded due to the reduction in fringing field length. With the theoretical parameters optimized for beamwidth enhancement, the proposed antenna was designed and compared, as shown in Fig. 4(a). Both the reference patch and the proposed antenna were designed with identical ground plane sizes, and the final parameters for the proposed antenna were obtained through multiple parametric analyses.

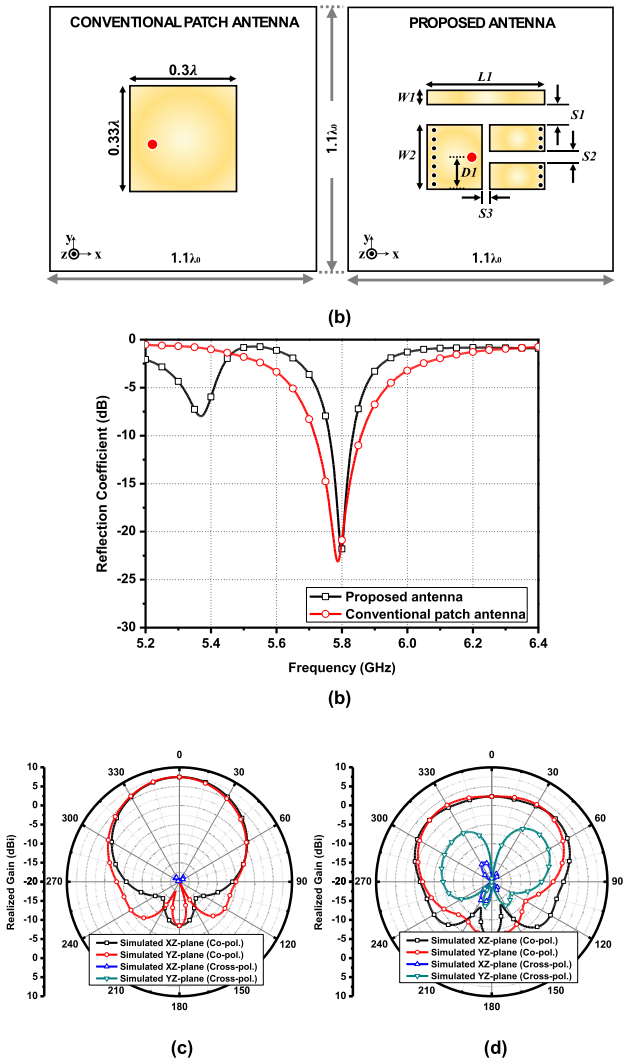

FIGURE 4. Conventional and proposed antenna with (a) geometric parameters (W1= 4 mm, W2= 9.8 mm, L1= 17.34 mm, S1= 3 mm, S2= 1.4 mm, S3= 1.2 mm, D1= 4.9 mm), and (b) simulated reflection coefficient, and simulated radiation pattern of (c) conventional antenna and (d) proposed antenna at 5.8 GHz.

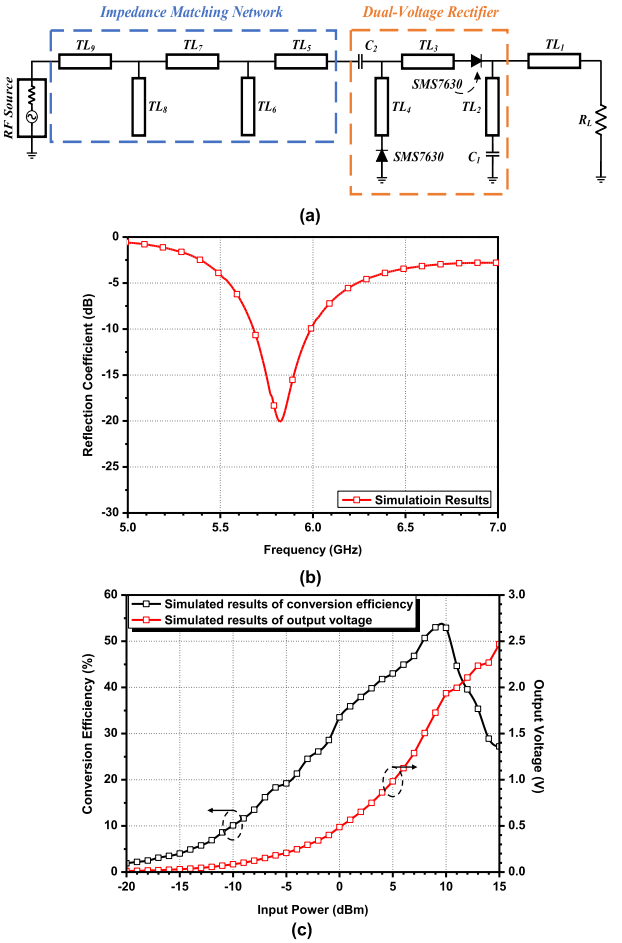

FIGURE 5. Proposed rectifier with matching network. (a) prototype view (C1=100 pF, C2=100 pF, RL=1000 Ω), (b) simulated reflection coefficient of rectifier, (c) simulated output voltage and conversion efficiency results of rectifier.

The reflection coefficients of both the conventional patch and the proposed antenna are shown in Fig. 4(b), with both antennas exhibiting a center frequency of 5.8 GHz, as intended. The simulated radiation patterns of the conventional patch antenna and proposed antenna are presented in Fig. 4(c) and (d). Wherein, the simulated HPBWs of conventional patch antenna are only about 78° in both xz and yz planes. However, the simulated HPBWs of the proposed antenna in the xz and yz planes were 154.6° and 137.1°, respectively, demonstrating an enhanced beamwidth.

B. DESIGN OF RF-DC RECTIFIER

In this paper, a 5.8 GHz RF-to-DC rectifier circuit with a dual-voltage rectifier structure was designed using Cadence AWR software, as shown in Fig. 5(a). The dual-voltage rectifier consists of two diodes and two capacitors. During the negative half cycle of the incident EM waves, diode D2 is on, while diode D1 is off, allowing charges to accumulate in capacitor C1. During the positive half cycle, diode D1 is on, while diode D2 is off, causing charges to accumulate in capacitor C2. Additionally, the charges from C1 flow to C2, effectively doubling the total charge and voltage in C2. Compared to a single-diode rectifying circuit, the dual-voltage rectifier can rectify both the positive and negative half cycles of the EM waves. Furthermore, the performance of the dual-voltage rectifier is enhanced by its higher breakdown voltage, providing greater capability to handle input power. Selecting the appropriate diode is crucial to further improving

TABLE 1. parameters of proposed rectifier.

Parameters	Width/Length (mm)	Parameters	Width/Length (mm)
TL_1	1.12/4.5	TL_6	1.12/4.66
TL_2	1.12/2	TL_7	1.12/2.3
TL_3	1.2/2	TL_8	1.12/0.61
TL_4	0.6/3.49	TL_9	1.12/2.5
TL_5	1.12/2.4		

the rectifier circuit's performance, considering factors like power loss, breakdown voltage, and biasing voltage. The Schottky diode SMS7630, a commercially available product from Skyworks, was chosen for achieving better system efficiency due to its low forward biasing voltage and the use of lumped capacitors. To account for dynamic changes in the rectifier's input impedance as frequency, input power, and load resistance vary, a matching network was incorporated. As mentioned in the previous section, the matching network consists of two short stubs, L1 and L3, which are designed to match the circuit to 5.8 GHz. The latter part of rectifier circuit includes the dual-voltage rectifier, which is composed of two Schottky diodes, two chip capacitors (C1 and C2), and a load resistor (R_L) at the end of the circuit. The designed parameters of rectifier are given in table 1. In addition, the simulated reflection coefficient is shown in Fig. 5(b). It is illustrated that the measured 10-dB impedance bandwidth ranges from 5.56 GHz to 5.84 GHz, covering the operating frequency of 5.8 GHz. According to the simulation results, the rectifier output voltages are recorded in terms of different RF input power. By utilizing the Efficiency function in AWR, the RF-to-DC conversion efficiency are calculated and shown in Fig. 5(c).

III. FABRICATION AND MEASUREMENT

A. FPR FABRICATION AND MEASUREMENT

The proposed wide-coverage antenna was implemented, where the total size of it is 60 mm × 60 mm × 5 mm. Fig. 6(a) shows the photos of proposed antenna from top and back view. The simulated and measured reflection coefficient results are shown in Fig. 6(b), with the 10-dB impedance bandwidth ranging from 5.81 GHz to 5.89 GHz, still encompassing the operating frequency of 5.8 GHz. The characteristic of wide reception ability is initially verified by measuring the beam pattern of proposed antenna. Fig. 6(c) and (d) show the measured and simulated beam pattern of proposed antenna, which indicates that the HPBWs are 155° and 137° in xz and yz planes respectively. The proposed wide-coverage FPR was implemented by integrating the rectifier circuit on the back side of the wide beamwidth antenna, maintaining the total thickness of the rectenna substrate, as illustrated in Fig. 7(a). Since the proposed FPR demonstrates good performance from an RF perspective, its practical performance in WPT applications must also be verified. The signals receiving ability of proposed rectenna has also been verified. Considering about the realistic application of the antenna, 1.5 m distance between transmitting antenna and receiving antenna is determined, at where the measurement of rectenna is in the far-filed region of the transmitting and the receiving antennas. At the transmitting side, RF signals are generated from vector signal generator E4438C and radiated by a 5.8 GHz single patch antenna. The PMI linear motion systems are used to place the transmitting antenna functioning as a device to steer the angle of the transmitting antenna. At the receiving side, the fabricated rectenna is placed and

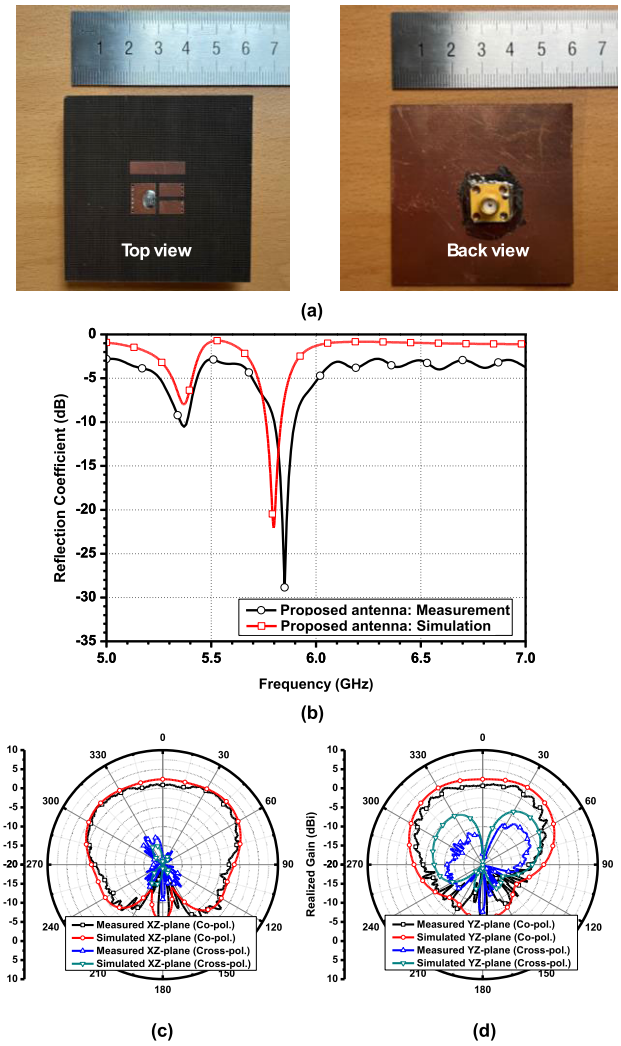

FIGURE 6. Proposed wide beamwidth antenna with (a) fabrication photo, (b) measured and simulated reflection coefficient, (c) and (d) measured and simulated beam patterns of proposed antenna.

connected to the spectrum analyzer. The photograph of the experimental environment is shown in Fig. 7(a). Based on the Friis transmission equation,

$$\frac{P_r}{P_t} = e_t e_r \frac{\lambda^2 D_t(\theta_t, \phi_t) D_r(\theta_r, \phi_r)}{(4\pi R)^2} \tag{6}$$

where P_t is the transmitted power from the patch antenna, and P_r is the received power of fabricated rectenna. P_r can also be expressed as,

$$P_r = P_t \frac{\lambda^2 G_r G_t(\theta_t)}{(4\pi R)^2} \tag{7}$$

where G_t and G_r are the gain of the transmitting antenna and the receiving antenna, R is the distance between transmitting antenna and receiving antenna. As RF energy signals are received by rectenna, the RF-to-DC conversion efficiency can be calculated based on energy conversion efficiency, which is

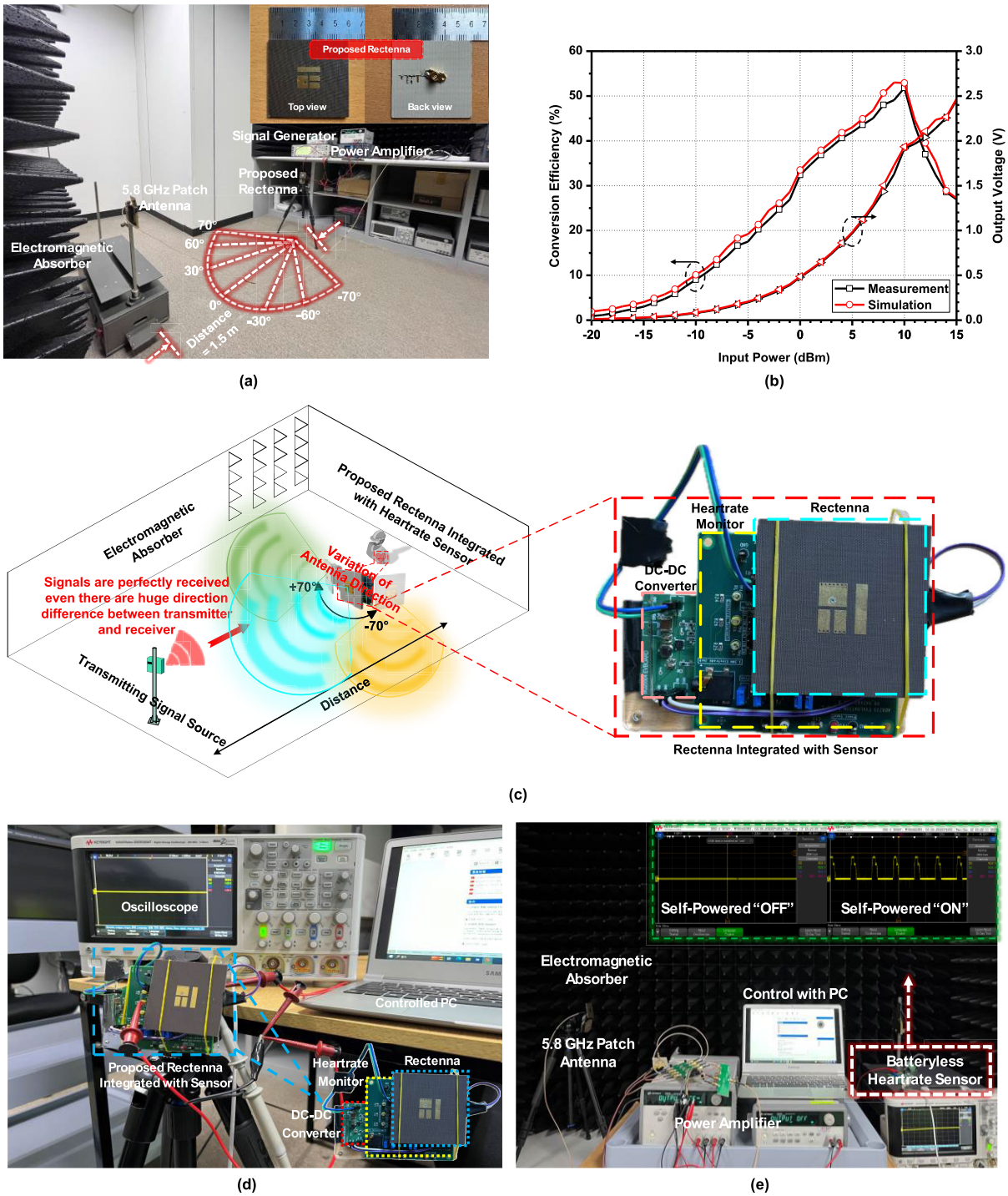

FIGURE 7. (a) Rectenna measurement setup, (b) measured and simulated results of rectenna for RF-to-DC performance, (c) diagram of integrated wireless powered sensor experiments, (d) experiment setup for the self-powered heartrate sensor, (e) measurement results.

express as,

$$\eta = \frac{P_{DC}}{P_r} = \frac{V_{DC}^2}{R_L P_r} \tag{8}$$

where P_{DC} is DC output power of proposed rectifier, and P_r is the received RF power. V_{DC} is the output voltage, and R_L is the load resistance. A power amplifier board is necessary, for a relatively large energy loss exists while RF signals are transmitting through 1.5 m long distance. The amplified RF rectenna is placed at the receiving side with proper polarization matching and a 1000 Ω load resistance. The multimeter is used to get the DC voltage of the output port. Based on expression (8), the measured and simulated results are depicted in Fig. 7(b) by sweeping the input power

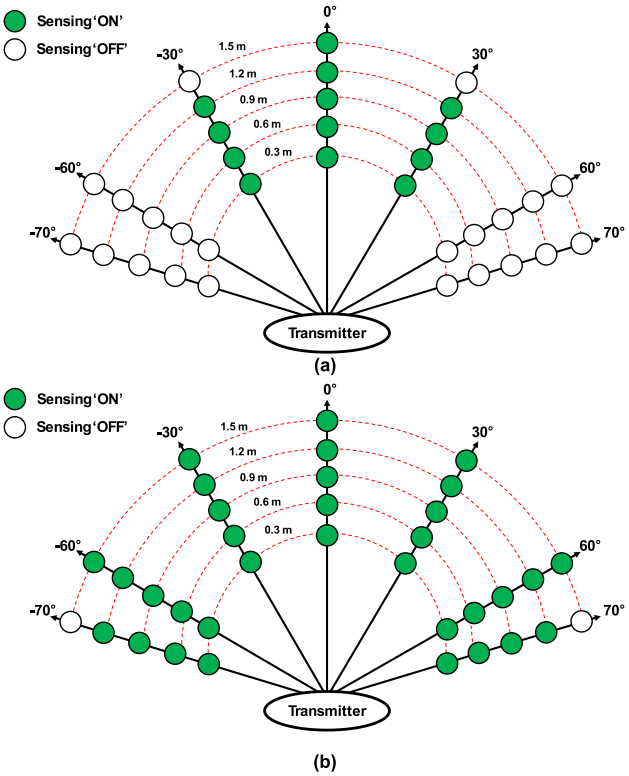

FIGURE 8. Measured wireless-powered sensor operation angles of (a) conventional patch rectenna and (b) proposed FPR integrated heartrate monitors.

of the rectenna from - 20 dBm to 15 dBm, where the output voltage of the rectenna with different input power, and the RF-to-DC conversion efficiency with different input power are included. It is illustrated that the measured maximum conversion efficiency is up to 51.8% with a 1.915 V output voltage when the input power is assigned as 10 dBm, which demonstrates that there is a favorable agreement between simulation and measurement is achieved.

B. WI0RELESS-POWERED SENSOR TEST WITH THE PROPOSED FPR

To demonstrate the operation of the self-powered sensor applications as depicted in Fig. 2, the proposed FPR was integrated with a commercially available heart rate monitor (AD8233), as shown in Fig. 7(c). In this setup, the proposed FPR was utilized as the energy receiver for the heart rate monitoring sensor, making it batteryless. By virtue of its wide-angle reception capability and compact size, the self-powered heart rate sensor could operate stably regardless of the physical orientation of the sensor or the angle of the incident RF signal. Fig. 7(d) and (e) show the experimental setup for the self-powered heart rate sensor, as well as the on and off status verification through an oscilloscope. Due to restrictions on testing with a human body directly, the test pulse was instead generated using an ECG generator. When RF energy was converted to DC power to supply the heart rate sensor, the generated pulse was detected and displayed on the oscilloscope, as shown in Fig. 7(e).

To evaluate self-powered sensor coverage, the PMI linear motion rotator was used to sweep the angle between the transmitting antenna and the self-powered heart rate sensor. The transmitting antenna was initially positioned at 0° on the horizontal azimuth plane. It was then rotated clockwise until the azimuth angle between it and the sensor under test reached 90°. Afterward, the transmitting antenna rotated counter-clockwise, repeating the above process. Additionally, the distance between the RF power source and the self-powered sensor was varied from 0.3 m to 1.5 m. Finally, Fig. 8(a) and (b) illustrate the operating range of the wireless-powered sensor for both a conventional rectenna and the proposed FPR-integrated heart rate sensor, respectively. The proposed FPR, when integrated with the sensor, was able to receive power even with a directional difference of up to ±70° relative to the RF source. In contrast, the conventional rectenna ceased operation when the directional difference exceeded ±30°. Therefore, the proposed rectenna demonstrates an excellent ability to receive RF power over a wide reception range, thereby offering greater flexibility in device movement and physical orientation.

IV. CONCLUSION

Earlier research on wide coverage rectennas often required either a large physical size or a compromise in rectenna gain to achieve improved coverage. In contrast, the proposed FPR offers a more compact design while maintaining consistent and stable gain across the entire hemispherical area. The proposed FPR also achieves a maximum RF-to-DC conversion efficiency of up to 51.8%. To validate its energy harvesting performance, the proposed FPR was integrated with a batteryless heart rate sensor. The self-powered sensor, equipped with the proposed FPR, demonstrated an extension of the coverage angle by more than 80° compared to conventional patch-based self-powered sensors. These results highlight the potential of the proposed FPR as a promising candidate for emerging energy harvesting system applications.

REFERENCES

[1] H. Satow, E. Nishiyama, and I. Toyoda, "A 5.8-GHz E-plane wide angle rectenna using magicts," *IEICE Trans. Commun.*, vol. J99, no. 6, pp. 415–423, Jun. 2016.
[2] H. Satow, Y. Tanaka, E. Nishiyama, and I. Toyoda, "An H-plane wide-angle rectenna using an in-phase/anti-phase dual-feed antenna," in *Proc. Int. Symp. Antennas Propag. (ISAP)*, Okinawa, Japan, Oct. 2016, pp. 532–533.
[3] T. P. Phyoe, H. Satow, E. Nishiyama, and I. Toyoda, "A dual-axis wide-angle rectenna using a triple-feed array antenna," in *Proc. Int. Symp. Antennas Propag. (ISAP)*, Phuket, Thailand, Oct. 2017, pp. 1–2.
[4] H. Satow, Y. Tanaka, E. Nishiyama, and I. Toyoda, "Design of an in-phase/anti-phase triple-feed array antenna using two types of magic-ts," *IEICE Commun. Exp.*, vol. 5, no. 11, pp. 413–417, 2016.
[5] D.-J. Lee, S.-J. Lee, I.-J. Hwang, W.-S. Lee, and J.-W. Yu, "Hybrid power combining rectenna array for wide incident angle coverage in RF energy transfer," *IEEE Trans. Microw. Theory Techn.*, vol. 65, no. 9, pp. 3409–3418, Sep. 2017.
[6] E. Vandelle, P. L. Doan, D. H. N. Bui, T. P. Vuong, G. Ardila, K. Wu, and S. Hemour, "High gain isotropic rectenna," in *Proc. IEEE Wireless Power Transf. Conf. (WPTC)*, Taipei, Taiwan, May 2017, pp. 1–4.

[7] Z. Liu, P. Wu, and G. Li, "A multibeam and surface plasmonic clothing with RF energy-localized harvester for powering battery-free wireless sensor," *IEEE Internet Things J.*, vol. 9, no. 15, pp. 13955–13964, Aug. 2022.
[8] M. Kumar, S. Kumar, A. Sharma, V. K. Malav, and P. Rattanpal, "An orthogonally polarized multibeam rectenna system to imitate isotropic DC pattern for orientation-insensitive microwave power delivery," *IEEE Trans. Compon., Packag., Manuf. Technol.*, vol. 14, no. 4, pp. 659–668, Apr. 2024.
[9] S. Kim, H.-W. Jo, J.-W. Kim, J.-I. Oh, J.-W. Yu, and B. Ahn, "Curved-retrodirective beamforming system to improve microwave power transmission efficiency in the Fresnel region," *IEEE Internet Things J.*, vol. 10, no. 17, pp. 15012–15024, Sep. 2023.
[10] H. Sun, S. Zhu, R. Ren, H. Zhang, and X. Ma, "Optimization of wireless power transmission under nonuniform incident power density distribution," *IEEE Antennas Wireless Propag. Lett.*, vol. 23, pp. 39–43, 2024.
[11] W. Zhang, J. Zhang, C. Song, R. Pei, X. Zhang, H. Liu, C. Han, Y. Huang, and J. Zhou, "Aperture sharing metasurface-based wide-beam antenna for energy harvesting," *AEU - Int. J. Electron. Commun.*, vol. 173, Jan. 2024, Art. no. 155009.
[12] Y. M. Afify, A. Allam, A. Tanemasa, and A. B. Abdel-Rahman, "Wideband circularly polarized antenna with enhanced gain and wide beamwidth for energy harvesting applications," in *Proc. 16th Eur. Conf. Antennas Propag. (EuCAP)*, Madrid, Spain, Mar. 2022, pp. 1–5.
[13] Y.-B. Kim, H.-J. Dong, K.-S. Kim, and H. L. Lee, "Compact planar multipole antenna for scalable wide beamwidth and bandwidth characteristics," *IEEE Trans. Antennas Propag.*, vol. 68, no. 5, pp. 3433–3442, May 2020.
[14] Y.-B. Kim, S. Lim, and H. L. Lee, "Electrically conformal antenna array with planar multipole structure for 2-D wide angle beam steering," *IEEE Access*, vol. 8, pp. 157261–157269, 2020.
[15] C. A. Balanis, *Antenna Theory: Analysis and Design*, 2nd ed., Hoboken, NJ, USA: Wiley, 2001.

YAN HAN received the B.S. degree in electronic and information engineering from Chongqing University of Technology, Chongqing, China, in 2023. He is currently pursuing the M.S. degree in intelligent semiconductor engineering with Chung-Ang University, Seoul, South Korea. His research interests include self-powered sensor-integrated smart antenna systems and RF circuit design.

EUNJI KIM received the B.S. degree in electrical engineering from Daegu University, Gyeongsan, South Korea, in 2023. She is currently pursuing the M.S. degree in intelligent semiconductor engineering with Chung-Ang University, Seoul, South Korea. Her research interests include wide-angle antennas and antenna-integrated module design.

HAN LIM LEE (Member, IEEE) received the B.A.Sc. degree in electronics engineering from Simon Fraser University, BC, Canada, in 2008, and the M.S. and Ph.D. degrees in electrical engineering from KAIST, Daejeon, South Korea, in 2010 and 2014, respectively. From 2014 to 2015, he was a Senior Engineer with the DMC Research Center, Samsung Electronics. In 2015, he joined the School of Electrical and Electronics Engineering, Chung-Ang University, where he is currently an Associate Professor. His research interests include microwave/RF circuits and communication systems, mmWave beamforming antennas and phased array systems, antenna-in-package (AiP), RFIC/MMIC, thermally effective RF design, microwave wireless power transmission (MWPT), RF energy harvesting, and sensor embedded smart antenna systems.